Optical phase conjugation (OPC)-assisted isotropic focusing

Mooseok Jang,[1,*] Anne Sentenac,[2] and Changhuei Yang[1,3]

[1]*Electrical Engineering, California Institute of Technology, 1200 E California Boulevard, Pasadena, California 91125, USA*
[2] *Institut Fresnel, CNRS, Aix-Marseille Université, Ecole Centrale Marseille, Campus de St. Jérôme, 13013 Marseille, France*
[3] *Bioengineering, California Institute of Technology, 1200 E California Boulevard, Pasadena, California 91125, USA*
[*]*mjang@caltech.edu*

Abstract: Isotropic optical focusing – the focusing of light with axial confinement that matches its lateral confinement, is important for a broad range of applications. Conventionally, such focusing is achieved by overlapping the focused beams from a pair of opposite-facing microscope objective lenses. However the exacting requirements for the alignment of the objective lenses and the method's relative intolerance to sample turbidity have significantly limited its utility. In this paper, we present an optical phase conjugation (OPC)-assisted isotropic focusing method that can address both challenges. We exploit the time-reversal nature of OPC playback to naturally guarantee the overlap of the two focused beams even when the objective lenses are significantly misaligned (up to 140 microns transversely and 80 microns axially demonstrated). The scattering correction capability of OPC also enabled us to accomplish isotropic focusing through thick scattering samples (demonstrated with samples of ~7 scattering mean free paths). This method can potentially improve 4Pi microscopy and 3D microstructure patterning.

References and links

1. S. W. Hell, "Far-Field optical nanoscopy," Science **316**(5828), 1153–1158 (2007).
2. S. W. Hell, R. Schmidt, and A. Egner, "Diffraction-unlimited three-dimensional optical nanoscopy with opposing lenses," Nat. Photonics **3**(7), 381–387 (2009).
3. J. Pawley, *Handbook of biological confocal microscopy* (Springer 2006).
4. D. G. Grier, "A revolution in optical manipulation," Nature **424**(6950), 810–816 (2003).
5. A. S. Nes, J. J. M. Braat, and S. F. Pereira, "High-density optical data storage," Rep. Prog. Phys. **69**(8), 2323–2363 (2006).
6. S. Hell and E. H. K. Stelzer, "Properties of a 4Pi confocal fluorescence microscope," J. Opt. Soc. Am. A **9**(12), 2159–2166 (1992).
7. K. Bahlmann, S. Jakobs, and S. W. Hell, "4Pi-confocal microscopy of live cells," Ultramicroscopy **87**(3), 155–164 (2001).
8. C. Sheppard and C. Cogswell, "Optics in medicine, biology and environmental research, edited by G. v," Bally Elsevier, 310–315 (1993).
9. M. Gu and C. J. R. Sheppard, "Three-dimensional transfer functions in 4Pi confocal microscopes," J. Opt. Soc. Am. A **11**(5), 1619–1627 (1994).
10. M. Born and E. Wolf, *Principles of optics* (Cambridge University Press 1998).
11. E. N. Leith and J. Upatnieks, "Holographic imagery through diffusing media," J. Opt. Soc. Am. **56**(4), 523–523 (1966).
12. A. Yariv, "Phase conjugate optics and real-time holography," IEEE J. Quantum Electron. **14**(9), 650–660 (1978).
13. Z. Yaqoob, D. Psaltis, M. S. Feld, and C. Yang, "Optical phase conjugation for turbidity suppression in biological samples," Nat. Photonics **2**(2), 110–115 (2008).

14. E. J. McDowell, M. Cui, I. M. Vellekoop, V. Senekerimyan, Z. Yaqoob, and C. Yang, "Turbidity suppression from the ballistic to the diffusive regime in biological tissues using optical phase conjugation," J. Biomed. Opt. **15**(2), 025004 (2010).
15. M. Cui and C. Yang, "Implementation of a digital optical phase conjugation system and its application to study the robustness of turbidity suppression by phase conjugation," Opt. Express **18**(4), 3444–3455 (2010).
16. E. Mudry, E. Le Moal, P. Ferrand, P. C. Chaumet, and A. Sentenac, "Isotropic diffraction-limited focusing using a single objective lens," Phys. Rev. Lett. **105**(20), 203903 (2010).
17. M. Cui, E. J. McDowell, and C. Yang, "An in vivo study of turbidity suppression by optical phase conjugation (TSOPC) on rabbit ear," Opt. Express **18**(1), 25–30 (2010).
18. P. Török, P. D. Higdon, and T. Wilson, "On the general properties of polarised light conventional and confocal microscopes," Opt. Commun. **148**(4-6), 300–315 (1998).
19. H. J. van Staveren, C. J. M. Moes, J. van Marie, S. A. Prahl, and M. J. C. van Gemert, "Light scattering in Intralipid-10% in the wavelength range of 400-1100 nm," Appl. Opt. **30**(31), 4507–4514 (1991).
20. M. Müllenborn, H. Dirac, and J. W. Petersen, "Three-dimensional nanostructures by direct laser etching of Si," Appl. Surf. Sci. **86**(1-4), 568–576 (1995).
21. G. von Freymann, A. Ledermann, M. Thiel, I. Staude, S. Essig, K. Busch, and M. Wegener, "Three-dimensional nanostructures for photonics," Adv. Funct. Mater. **20**(7), 1038–1052 (2010).
22. M. C. Lang, T. Staudt, J. Engelhardt, and S. W. Hell, "4Pi microscopy with negligible sidelobes," New J. Phys. **10**(4), 043041 (2008).

1. Introduction

Optical focusing is important for a broad range of applications, such as biological imaging [1–3], particle trapping [4], and optical data storage [5]. A focused light beam can typically achieve diffraction-limited transverse spot size through the use of broadly available microscope objective lenses. Interestingly, the axial focused spot size tends to be 3-5 times worse. This is attributable to the fact that single-sided optical focusing can only bring at most a hemisphere's worth of optical k-vector (spatial frequency) components to the focused spot – sufficient to create a tight transverse focus but insufficient to achieve the same along the optical axis (Fig. 1(a)). In the context of focused-beam scanning microscopy, such as confocal microscopy, this translates to a superior transverse resolution but a poor axial resolution.

Isotropic focusing can address this limitation by bringing in a full angular range of optical k-vector components which results in diffraction-limited spot size along all axes. Conventionally, isotropic focusing is achieved by employing two high numerical aperture (NA) objective lenses facing each other (Fig. 1(b)). This approach was originally proposed and demonstrated in conjunction with confocal imaging system [6–9]. The imaging technique, so called 4Pi microscopy, improves an axial resolution 3-5 times compared to the conventional focusing technique with a single objective lens [3, 6, 9, 10]. However, the broader applications of 4Pi microscopy are limited by the following challenges. 1) The two objective lenses need to be precisely aligned so that their focused spots overlap exactly, 2) optical aberrations (including sample scattering) in the intervening medium between the two objective lenses can disrupt the focus overlap or, worse, deteriorate either one or both of the focused beams so that the light beam(s) no longer come to the focus. This second challenge is especially problematic and restricts 4Pi imaging application to thin sample sections (~50 microns).
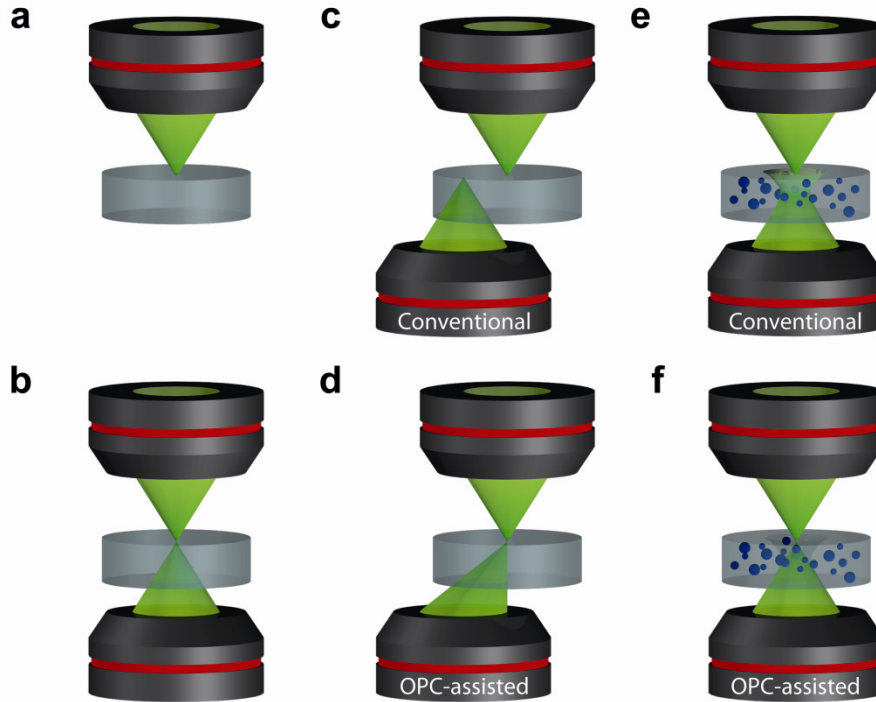
Fig. 1. (a) Conventional unidirectional focusing scheme with single lens. (b) Conventional isotropic focusing scheme with two aligned lenses. The aperture angle (contributing k-vector components) for the focused light beam is doubled in the isotropic focusing scheme. (c-f) Conventional and OPC-assisted isotropic focusing in two circumstances – (c and d) with lateral misalignment (e and f) and through inhomogeneous media. The conventional system fails to maintain isotropic focusing for both cases, while the OPC-assisted system adaptively corrects the aberrations.

In this work, we report the application of optical phase conjugation (OPC) in an isotropic focusing scheme. Optical phase conjugation (OPC) is the process by which an incoming light field is recorded and a phase sign-reversed copy of the light field is generated and played back. In effect, it can be interpreted as a time-reversed reflection process as the phase-conjugated field will propagate back along the original trajectory [11–15]. One research group recently showed that the time-reversal theory can be employed in non-adaptive way to achieve isotropic focusing simply with a single objective lens and a plane mirror [16]. However, this modification does not mollify the optical aberration challenge. In addition, while this approach eliminates the need for precise alignment of the objective lens pair, it still requires precision in mirror placement unless some form of feedback is employed. The new OPC-based approach described in this paper can dynamically overcome the abovementioned challenges.

In OPC-assisted isotropic focusing, we use the first objective lens to focus light at the desired location in the target medium. The transmitted wavefront is then collected by the second objective lens and recorded by an OPC system. The OPC system then generates a phase conjugated beam (OPC beam) back through the second objective lens. The OPC beam will retrace the original trajectory in a time reversed fashion, and thereby guarantees that it will exactly overlap with the focused beam from the first objective lens. The automatic alignment inherent in this technique resolves the first challenge. This makes isotropic focusing more robust. Additionally, the OPC beam automatically corrects for sample aberrations and therefore resolves the second challenge. To date, these have not been

accomplished by other technologies. We invite readers to examine Fig. 1 for a pictorial illustration of advantages described here.

In this paper, we report experimental demonstration of OPC-assisted isotropic focusing and showed that this scheme can indeed tackle these two abovementioned challenges - with misalignment between two objective lenses and through scattering sample. Conventional isotropic focusing method will fail to create an isotropic focused spot in both cases (Figs. 1(c) and 1(e)). With an aid of OPC, we experimentally showed that isotropic focusing can be achieved even with misalignment up to 140 microns and 80 microns along transverse and axial direction, respectively (Fig. 1(d)). We also demonstrated that isotropic focusing can be achieved in a scattering media with $\mu_s l \sim 7$, where μ_s is scattering coefficient and l is medium thickness (Fig. 1(f)). Therefore, this isotropic focusing approach can potentially allow 4Pi microscopy to image thicker and inhomogeneous tissue sections. Amongst the other applications, this approach may also enable high-resolution laser-etching of 3D microstructure.

2. Result

2.1 Implementation of OPC-assisted isotropic focusing

Our implementation of OPC-assisted isotropic focusing involved the incorporation of a digital optical phase conjugation (DOPC) into the conventional isotropic focusing scheme (see Fig. 2). The DOPC technique is an established optoelectronic approach for the measure of an input light field and the play back of an optical phase conjugated light field [14, 15, 17]. In brief, we first focused light into a target medium through the first objective lens (OBJ1) of the pair (UPLFLN 100XO2, Olympus, oil immersion type, NA 1.3). The transmitted light was then collected by the second objective lens (OBJ2) and its wavefront was measured and played back by a DOPC system. The employed DOPC system can complete a cycle of measurement and playback in less than a second and it had the capability to control many number of optical modes (up to 10^6, a measure of the playback quality, see Ref. 13 for more information). The playback can be maintained for an arbitrarily long time.

The DOPC system consisted of a camera arranged to perform interferometry based wavefront measurement (SCMOS camera, PCO), a spatial light modulator (phase-only modulating LCoS, Holoeye), and an optical phase modulator (ElectroOptic Modulator, Thorlabs) for phase-shifting interferometry [15, 17]. We used a 1× telescope to optically conjugate the DOPC system to the back aperture of objective lens (OBJ2) to optimize OPC effectiveness. This system is similar to the one described in Ref. 15. Readers interested in more experimental details regarding the system are invited to examine Ref. 15.

We further built a conventional confocal fluorescence detection setup to examine the focused light distribution characteristics. A CCD camera (pixelfly qe, PCO) was also installed to allow observation of the transverse light distribution generated from OBJ2, though it was not a necessary component of the confocal setup. Finally, we used a nanopositioning stage (P-611.3, Physik Instrumente) to actuate the sample as need, such as when we perform raster-scanning of fluorescent bead.
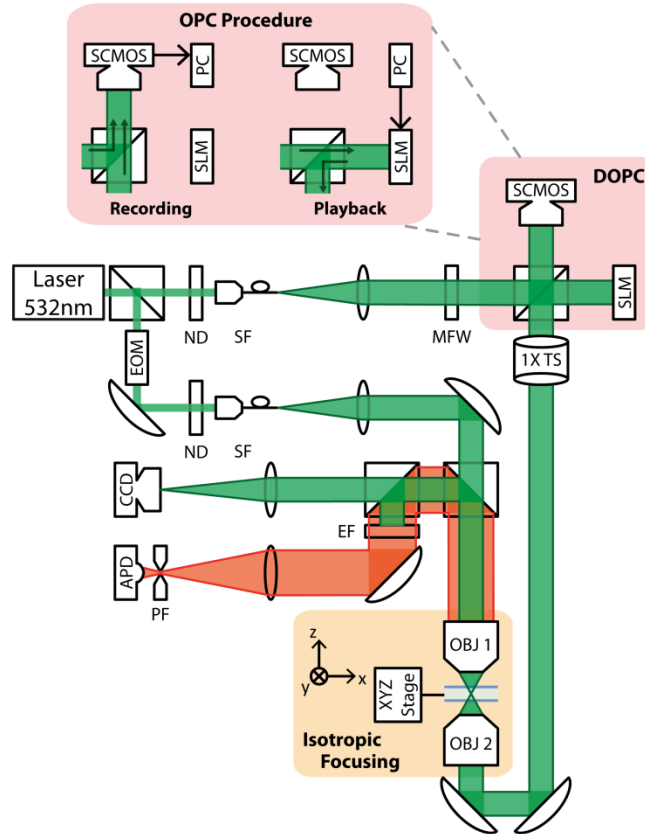
Fig. 2. Schematic diagram of the OPC-assisted isotropic focusing system. 532nm laser beam was split into two paths. Both beams were spatially filtered as coupled to single mode fiber and collimated by bulk lenses. One path passing EOM formed an original focal spot through OBJ1 and entered DOPC system, the other path was split into two beams – a reference beam for phase-shifting holography and an OPC beam retracing the original focal spot back. ND, continuous neutral density filter; SF, spatial filter; 1X TS, 1X telescope; PH, pinhole; MFW, motorized filter wheel; OBJ, objective lens; EOM, Electro-optical phase modulator; SLM, spatial light modulator; SCMOS, scientific CMOS camera; CCD, CCD camera; APD, avalanche photo diode.

We characterized the focused spot size by raster-scanning an isolated fluorescent bead (diameter $100\,nm$) across the focal region. The bead was embedded in anti-fade reagent (~80 microns thick, refractive index = 1.46, Invitrogen) which was sandwiched between two coverslips ($170\,\mu m$ thick, refractive index = 1.515). A solid-state laser $532\,nm$ laser served as the light source. We picked off the fluorescence emission collected by OBJ1 via a 50/50 beam splitter and confocally detected the signal with a spectral filter (LP02-561RS-25, Semrock) to eliminate the excitation light, a $10\,\mu m$ pinhole (set at the 0.8 Airy disk diameter) to reject the out-of-focus emission light, and an avalanche photodiode (APD) detector (SPCM-AQRH-14, Perkin Elmer) to detect the emission photons from the focal spot.
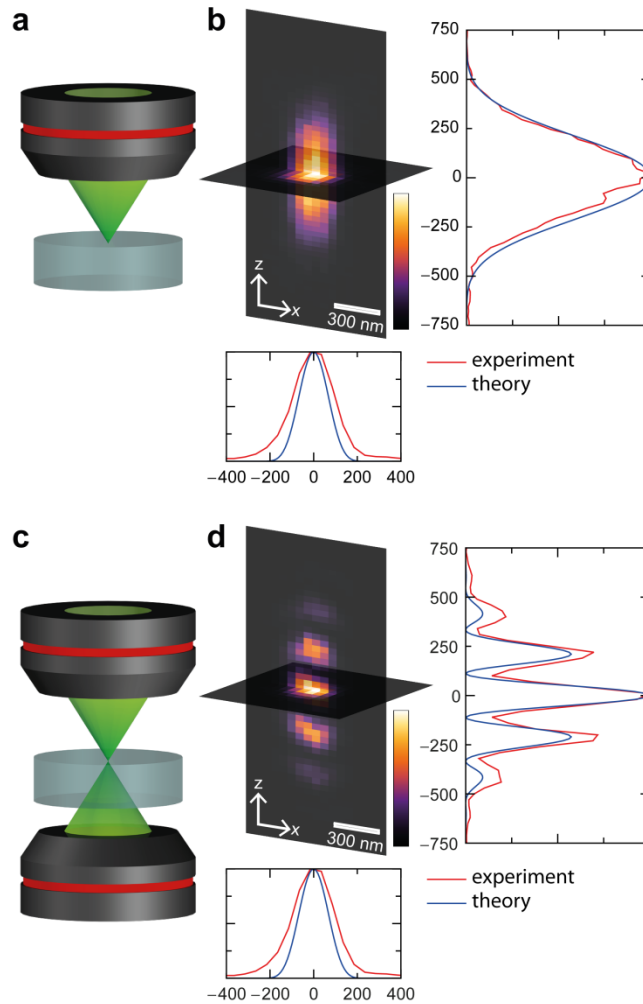
Fig. 3. PSF of unidirectional and isotropic focusing system. (a and c) Unidirectional and isotropic focusing schemes with single lens and two aligned lenses. (b and d) Transverse and longitudinal section of the measured PSF in conjunction with confocal detection system. 1D profiles presents the axial and transverse PSF. (red line: measured profile, blue line: theoretical profile). All graphs plotted on a micron scale.

The 3D scanning of single bead was performed through the following procedures: 1) We placed a fluorescent bead at the focal spot of OBJ1. 2) We measured the phase map of the wave front exiting OBJ2 by the means of phase shifting interferometry. 3) We then displayed the conjugated phase map on the SLM. 4) We alternately turned on only one of the beams to excite the fluorescent bead. We adjusted the power of the time-reversed beam so that the bead fluoresced with the same brightness for each of the beams. (A motorized filter wheel was used for this purpose.) 5) Next, we turned on both beams and adjusted the relative phase between two beams via the EOM to achieve constructive interference of the two focused light beams, which maximized the fluorescence signal from the bead. 6) Finally, we translated the specimen across the focal region to perform scanning. For this experiment, the excitation power of each beam was set at about $1\,\mu W$.

Through the raster-scan measurements, we were able to characterize the system point spread function (PSF), which is given by the product of the focused light distribution and

confocal detection PSF. For comparison, we also measured the PSF associated with unidirectional focusing (light was focused through the first objective lens (OBJ1) and the second objective lens (OBJ2) was blocked). In addition, we also computed the theoretical light distributions near the focal region for both geometries with the use of the vectorial ray tracing model [18].

We experimentally found that PSF for unidirectional focusing gave a spot size (full with at half maximum, FWHM) of $200\,nm$ and $500\,nm$ along transverse and axial direction, respectively (Figs. 3(a) and 3(b)). The axial spot size improved to $120\,nm$ when we activated OPC-assisted isotropic focusing (Figs. 3(c) and 3(d)). Unsurprisingly, we observed a characteristic interference of the two counter-propagating beams that resulted in a sharpened central peak surrounded by side lobes. The 1D intensity profiles showed relatively good agreements between the experimental PSF and the theoretical PSF. The discrepancy can be attributed to finite-sized pinhole and some aberration caused from refractive index mismatch between the embedding medium and cover slip.

2.2 Isotropic focusing through two misaligned lenses

To demonstrate that this scheme can robustly correct for misalignment of the objective lenses, we intentionally disrupted the foci overlap by misaligning the OBJ2 in the next set of experiments. In this situation, we expected the DOPC to robustly measure the transmitted wavefront (collected through OBJ2) and playback an appropriate phase conjugated copy of the wavefront and, thereby, preserve the beam overlap.

Figure 4 shows the transmitted wavefront recorded by the DOPC system when the objective lenses were misaligned. As the transverse and axial displacement ware increased, we observed fringe patterns and Bull's eye patterns, respectively, with higher spatial frequency components. We note that the light field experiences analogous wavefront distortion when the medium consists of multiple layers with different refractive indices or has a continuous gradient of refractive index.
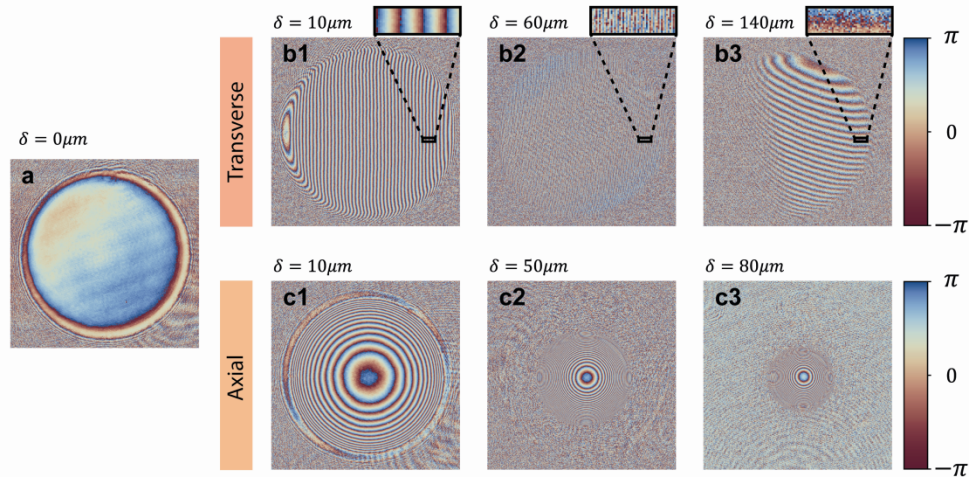

Fig. 4. Measured wave front (phase map) exiting transversely/axially misaligned objective lens (OBJ2 in Fig. 2). (a) Phase map of the wave front exiting well-aligned objective lens. Flat pattern (plane light beam) was observed. (b1-b3) Phase map of the wave front exiting transversely misaligned objective lens with an incremental displacement. Fringe patterns (angularly deviated light beam) with different frequency were detected. (c1-c3) Phase map of the wave front exiting axially misaligned objective lens with an incremental displacement. Bull's eye patterns (converging light beam) were emerged. With severe misalignment, some higher spatial frequency information was missed.
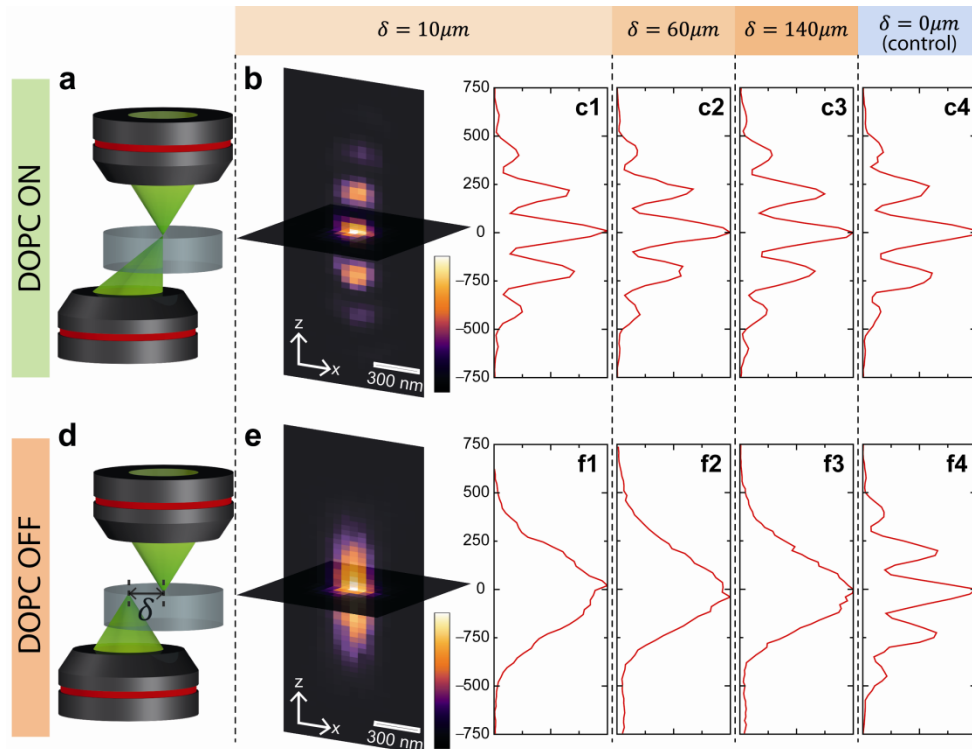
Fig. 5. PSF of OPC-assisted and conventional isotropic focusing system with a 10 microns transverse misalignment. (a and d) OPC-assisted and conventional isotropic focusing schemes. (b and e) Transverse and longitudinal section of the measured PSFs in conjunction with confocal detection system. (c1-c3) 1D axial PSFs of OPC-assisted isotropic focusing system with incremental transverse misalignment. The OPC-assisted system robustly provided the identical PSFs with marginal errors (FWHM of $120\,nm$). (f1-f3) 1D axial PSFs of conventional isotropic focusing system. As two objective lenses formed two far-distant foci, the system presented the elongated profile (FWHM of $500\,nm$). (c4 and f4) 1D axial PSFs of two systems with well-aligned objective lenses. As a control set of experiments, axially sharpened profiles were measured for both systems. All graphs plotted on a micron scale.

Figures 5(b) and 5(c) shows the measured PSFs associated with a 10 microns transverse misalignment of OBJ2. For the sake of comparison, we also plotted the PSFs without an aid of DOPC (Figs. 5(e) and 5(f)). With the use of OPC-assisted isotropic focusing, the PSF spot size was measured as $200\,nm$ and $120\,nm$ along transverse and optical axes, respectively. Without the correction, the system basically worked like a unidirectional focusing system because the two lenses formed focused spots that were too distant to overlap ($10\,\mu m$ apart). We repeated the experiment with 10 microns axial misalignment. The results are shown in Fig. 6.
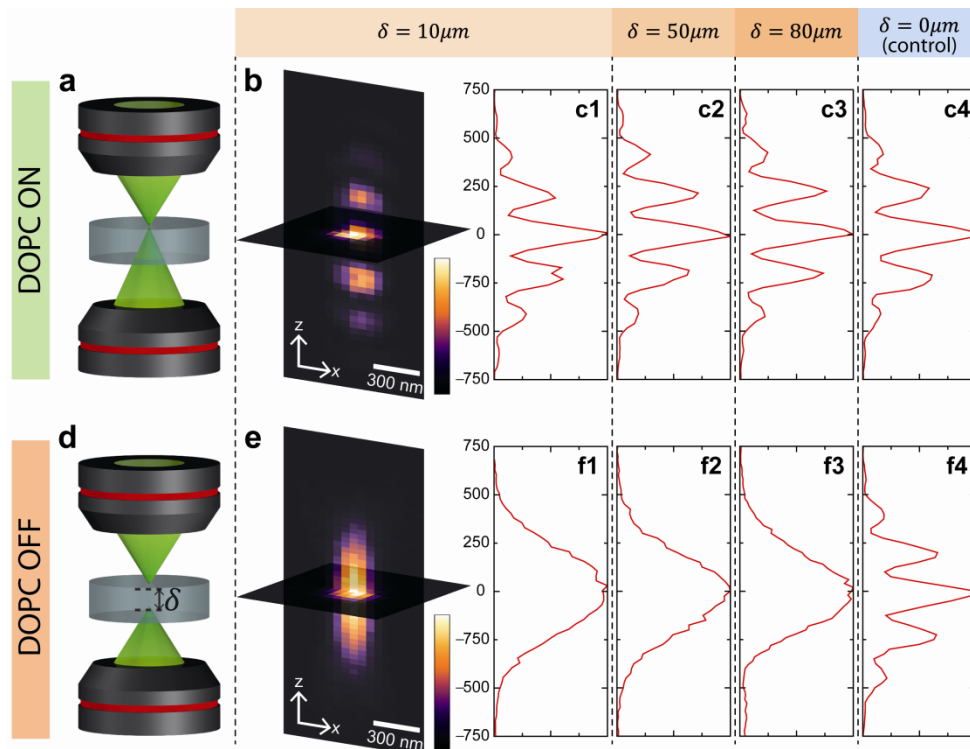
Fig. 6. PSF of OPC-assisted and conventional isotropic focusing system with a 10 microns axial misalignment. (a and d) OPC-assisted and conventional isotropic focusing schemes. (b and e) Transverse and longitudinal section of the measured PSFs in conjunction with confocal detection system. (c1-c3 and f1-f3) 1D axial PSFs of OPC-assisted isotropic focusing system and conventional isotropic focusing system with incremental axial misalignment. (c4 and f4) 1D axial PSFs of two systems with well-aligned objective lenses. All graphs plotted on a micron scale.

Practically, we expected that the compensable misalignment range would be largely set by the wavefront pixilation during DOPC play back. Intuitively speaking, the finite pixel size on the spatial light modulator (SLM) implied that its primary diffracted beam can only cover a finite angular range. At the objective lens's aperture stop, this maximum deflection angle equaled ~1.9 degree, which corresponded to ~60 microns transverse focal spot displacement. However, we experimentally found that it was actually possible to maintain isotropic focusing beyond this range by employing higher diffraction orders. We do note that the power transmission to the phase-conjugated focal spot will drop as the misalignment increases. This implied that we need to increase the play back power to compensate. We confirmed that our system was able to maintain isotropic focusing up to a misalignment of 140 microns transverse misalignment (Fig. 5(c)). This range can be further extended by increasing the playback power beyond our system's capability. Likewise, we were able to correct up to 80 microns axial misalignment (Fig. 6(c)) with our current setup. We expect that larger misalignments can be compensated if higher playback power is available.

2.3 OPC-assisted isotropic focusing through an optically inhomogeneous medium

To demonstrate that the OPC-assisted isotropic focusing method can robustly accomplish isotropic focusing through an optically inhomogeneous medium, we conducted the following experiment.

We prepared a 80 microns thick slab of scattering medium consisting of polystyrene beads (refractive index = 1.60, Polysciences) of various sizes (diameter

$100\,nm$, $100\,nm$, $350\,nm$, $500\,nm$, and $1\,\mu m$) corresponding to an anisotropy factors of 0.13, 0.53, 0.80, 0.89, and 0.96, respectively (calculated based on Mie theory). The mean number of scattering events was determined to be $\mu_s l \sim 7$ by the ballistic transmission measurement [19]. Fluorescent beads were embedded as well to provide PSF measurement targets.

We note that the distortion correction will only work for the play back beam. In other words, the fine focal spot needs to be created from the first objective lens (OBJ1) so that OPC beam retrace it from the opposite direction – this implies that the intervening medium between the first objective lens and the focal point would have to be of sufficiently low turbidity.

In this experiment, our focus was placed 10 microns into the medium (on OBJ1 side). Figure 7(a) shows the transmitted wavefront recorded by the DOPC system (on OBJ2 side). It presented the disordered pattern due to the multiple scattering. Unsurprisingly, the play back light was able to retrace its way through the scatterers and generate a good focal spot at the original focal region. Without the correction (plane light field from DOPC system), the light distribution was significantly disturbed (Figs. 7(b) and 7(c)). The measured PSF for both situations are presented in Figs. 8(b) and 8(d). Axial spot size of the PSF was enhanced to $120\,nm$ from $500\,nm$ with the aid of DOPC.
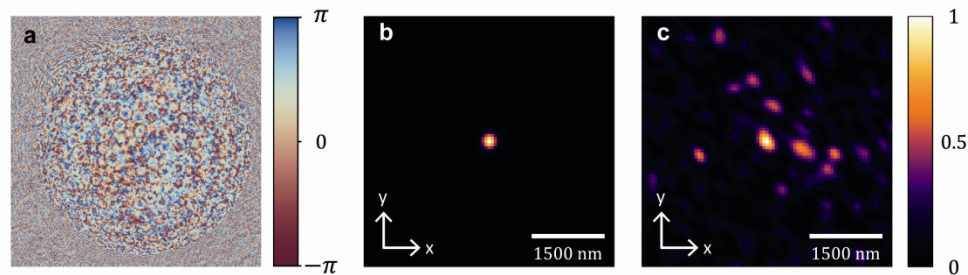

Fig. 7. (a) Measured wave front (phase map) propagated through an inhomogeneous media with $\mu_s l \sim 7$. As the light experienced multiple scatterings, disordered wave front was measured. (b-c) Light intensity distribution emerged from objective lens on the side of DOPC (OBJ2 in Fig. 2). Those were captured from additional CCD sensor through OBJ1 (Fig. 2). (b) With an aid of DOPC, sharp focal spot was reconstructed. (c) Without and aid of DOPC (plane light beam from DOPC), focal spot was significantly degraded.

If we translate the inhomogeneous medium to scan the spot through the region of interest, the phase-conjugated focal spot is gradually blurred [13, 14]. This is expected as the displacement of the sample implies a change in the scatterers configuration as seen by the DOPC system. Consequentially, DOPC needs to be performed for each different configuration of the scatterers. However, in the forward-scattering regime, which prevails in a few hundreds microns thick biological sample, phase-conjugated focal spot presents robustness to the sample displacement even up to a few micrometers [13]. In our experiment, OPC was only performed 4 times while collecting the 0.8 micron x 1.5 micron section image shown in Fig. 6(b).
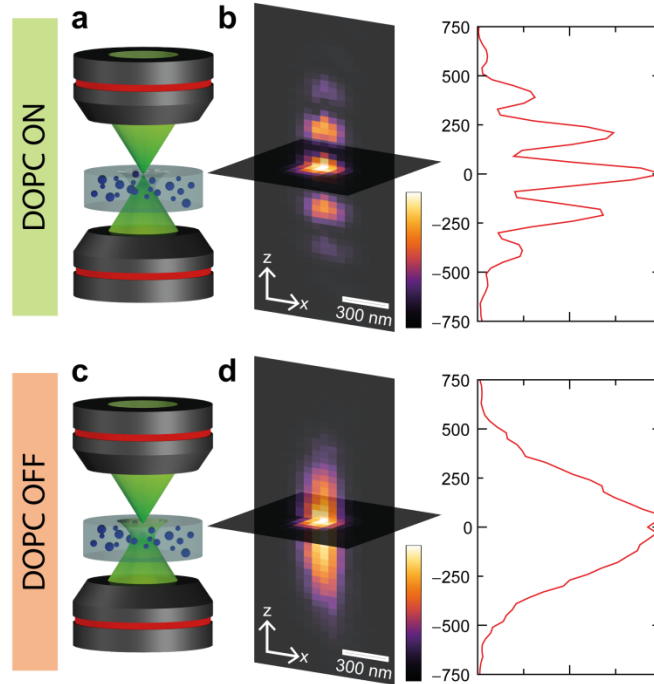
Fig. 8. PSF of OPC-assisted and conventional isotropic focusing system through the optically inhomogeneous media ($\mu_s l \sim 7$). (a and c) OPC-assisted and conventional isotropic focusing schemes. (b and d) Transverse and longitudinal section of the measured PSFs in conjunction with confocal detection system. 1D axial PSFs clearly showed the recovery of isotropic focusing with an aid of DOPC. All graphs plotted on a micron scale.

3. Discussion

In this study, we have developed a new adaptive focusing technique, termed OPC-assisted isotropic focusing. Our prototype system demonstrated that this approach is robust against objective lens misalignment (up to 140 microns transverse and 80 microns axial misalignment demonstrated) and is capable of creating an isotropic focus even in the presence of turbidity ($\mu_s l \sim 7$ demonstrated) on one side of the focal point. We believe that the method is directly relevant in two application areas – 4Pi microscopy and fabrication of 3D microstructure [6–9, 20].

In 4-Pi microscopy, this adaptive approach should allow more robust operations where exacting alignment of the objective lens pair can be significantly relaxed. The ability to work robustly with samples that are too turbid to image with conventional 4-Pi microscopy is another significant advantage. We note that this approach still requires the light beam from the first objective lens to be well focused, which implies that the intervening medium between the focus and the first objective lens needs to be relatively clear (same requirement as for conventional 4-Pi). However, the method will be able to accommodate turbidity associated with the other side of the focus. This implies that this new adaptive approach will likely be suitable for performing 4-Pi imaging of superficial cells or layers on a thick sample sections (such as fluorescently tagged proteins near the top or bottom of a developing embryo).

This adaptive focusing method can also address direct laser etching of 3D microstructures, such as photonic crystals. One feasible way to fabricate 3D microstructures would be to perform a focused laser beam scanning to etch planar patterns into a suitable slab of material [20]. By progressively etching and vertically compiling a vertical stack of planar patterns, we can arrive at a 3D microstructure. The use of isotropic focusing in this type of application can

ensure the diffraction-limited spatial resolution in 3 dimensions. However, conventional isotropic focusing is not a practical solution. Specifically, we can expect that as layers of planar pattern are progressively etched into the material, they will collectively behave like a scattering medium and will disrupt one of the focused beams. As we have reported above, OPC-assisted isotropic focusing will not suffer from this shortcoming. This advancement is likely to be highly relevant to 3D photonic crystal fabrication, as such structures do generally require features that are of the optical wavelength scale along all 3 axes [21].

Our current experimental setup is intended only as a demonstration of the adaptive focusing method's advantages. To translate the work for applications, it is highly desirable to suppress the side lobes surrounding the central peak. This can be achieved by switching to the two-photon excitation scheme or by employing higher NA objective lens [22]. It is also beneficial to improve the system's speed. We expect that the use of high speed sensor and digital micromirror device in place of scientific CMOS (SCMOS) camera and SLM will improve the DOPC process speed to $1000\,Hz$ (currently $\sim 5\,Hz$). On a different front, it will also be favorable to develop a more dynamic phase control method that can automatically lock the relative phase of the two counter-propagating beams such that optimal constructive interference can occur at the center of the focal spot.

Acknowledgments